Synthesis, characterization and photocatalytic activity of 1D TiO_2 nanostructures

Julieta Cabrera, Hugo Alarcón, Alcides López, Roberto Candal, Dwight Acosta and Juan Rodriguez

ABSTRACT

Nanowire/nanorod TiO_2 structures of approximately 8 nm in diameter and around 1,000 nm long were synthesized by alkaline hydrothermal treatment of two different TiO_2 nanopowders. The first precursor was TiO_2 obtained by the sol-gel process (SG-TiO_2); the second was the well-known commercial TiO_2 P-25 (P25-TiO_2). Anatase-like 1D TiO_2 nanostructures were obtained in both cases. The one-dimensional (1D) nanostructures synthesized from SG-TiO_2 powders turned into rod-like nanostructures after annealing at 400 °C for 2 h. Conversely, the nanostructures synthesized from P25-TiO_2 preserved the tubular structure after annealing, displaying a higher Brunauer–Emmett–Teller surface area than the first system (279 and 97 m^2/g, respectively). Despite the higher surface area shown by the 1D nanostructures, in both cases the photocatalytic activity was lower than for the P25-TiO_2 powder. However, the rod-like nanostructures obtained from SG-TiO_2 displayed slightly higher efficiency than the sol-gel prepared powders. The lower photocatalytic activity of the nanostructures with respect to P-25 can be associated with the lower crystallinity of 1D TiO_2 in both materials.

Key words | 1D TiO_2 nanostructures, hydrothermal treatment, photocatalytic activity

Julieta Cabrera
Hugo Alarcón
Alcides López
Juan Rodriguez (corresponding author)
Universidad Nacional de Ingeniería,
Lima,
Perú
E-mail: *jrodriguez@uni.edu.pe*

Alcides López
Instituto Peruano de Energía Nuclear,
IPEN, Lima,
Perú

Roberto Candal
INQUIMAE,
Facultad de Ciencias Exactas y Naturales,
Universidad de Buenos Aires,
Argentina

Dwight Acosta
Instituto de Física,
UNAM, México D.F.,
Mexico

INTRODUCTION

TiO_2 nanomaterial is well-studied and commonly used material for liquid and gas-phase applications due to its high performance as a photocatalyst for degradation of organics, water splitting and solar cells, among others (Ollis *et al.* 1991; Cowan *et al.* 2010; Yan & Zhou 2011; Ren *et al.* 2012). Under UV illumination, electrons from the TiO_2 valence band jump to the conductive band, leaving oxidant positive holes behind (Ibhadon & Fitzpatrick 2013). The electrons and holes diffuse to the surface of TiO_2 particles, where they can participate in oxidative-reduction processes (such as water oxidation, oxygen reduction, etc.). One of the main drawbacks of TiO_2 nanoparticles is the random pathway of the electrons during the photocatalytic reactions that may lead to hole-electron recombination, which increases with the presence of surface defects or trapping sites. The synthesis of particles with a large aspect ratio is an approach recently explored to increase the photoefficiency of TiO_2 (Lai *et al.* 2014). Over recent years, one-dimensional (1D) nanostructures (such as nanotubes, nanorods, nanowires, nanobelts, etc.) of inorganic materials have attracted considerable attention because they offer a larger surface area in comparison to nanoparticles (Yamin *et al.* 2012). In the case of TiO_2, the nanotubes exhibit unique properties that may be beneficial for photocatalysis. These unique features include: (i) enhanced light adsorption due to the high ratio length/diameter, (ii) rapid and long-distance electron transport capability, (iii) large specific surface area, and (iv) ion exchange ability (Liu *et al.* 2014). Different routes have been developed in order to create TiO_2-based 1D nanostructures such as the assisted-template method (Wu & Yu 2004; Maiyalagan *et al.* 2006), electrochemical anodic oxidation (Neupane *et al.* 2011) and hydrothermal treatment (Wang *et al.* 2008; Nakahira *et al.* 2010; Asiah *et al.* 2013). Hydrothermal treatment of TiO_2 particles in alkaline solutions is one of the simplest techniques to produce 1D-layered titanate structures. It is a simple wet chemical process, more favourable for large-scale reaction and production of low-cost material for the formation of TiO_2 nanotubes-nanorods compared to other methods, such as surfactant-assisted templating (Adachi *et al.* 2003; Liu *et al.* 2014). The hydrothermal synthesis of TiO_2 nanotubes involves several steps where the structure of the

doi: 10.2166/wst.2014.312

TiO_2 precursor changes completely. These steps include acid wash and thermal treatment. The nature of the TiO_2 used as the precursor in the alkaline hydrothermal synthesis affects the quality and properties of the final product (Liu *et al*. 2014). In this work, we report on the synthesis of rod and tube-like TiO_2 nanostructures created by hydrothermal synthesis using TiO_2 nanopowders synthesized in our laboratory by the sol-gel method and commercial TiO_2 P-25 as precursors. Their photocatalytic efficiency was compared by means of Rhodamine B (RhB) photocatalytic degradation.

MATERIAL AND METHODS

All reagents were used as received without further purification. Titanium isopropoxide, NaOH and HCl were purchased from Merck (New Jersey, USA). Commercial TiO_2 powder P25 was obtained from Degussa (Germany).

Synthesis and characterization of TiO_2 nanostructures

Nanotubes/nanorods were synthetized by hydrothermal treatment of 1 g of TiO_2 powder (commercial P25: P25-TiO_2, or sol-gel synthetized TiO_2: SG-TiO_2) in a 10 M NaOH solution at 130 °C for 18 and 24 h. After hydrothermal treatment, the obtained white powder was vacuum-filtered, washed with HCl solution for ionic exchange and then washed with distilled water until a neutral pH was reached. Finally, the samples were annealed at 400 °C for 2 h to crystallize the material.

In the synthesis of nanoparticles from the sol-gel method a colloidal solution was obtained by slowly adding drops of titanium isopropoxide to a vigorously stirred concentrated acidic solution (HCl 0.1 M) at room temperature. The resulting suspension was heated at 70 °C for 2 h to peptize the aggregates of particles and, in order to get the nanoparticles, it was auto-cleaved in a stainless steel chamber at 220 °C for 12 h. After the hydrothermal treatment, a transparent solution and a white precipitate was obtained. The white precipitate was washed and dried at 100 °C overnight in a dry oven.

The obtained nanostructures were characterized by X-ray diffraction (XRD) in a Rigaku diffractometer (Rigaku Corp., Japan) using CuKα radiation ($\lambda = 1.54056$ Å). The morphology was studied by field emission scanning electron microscopy (FE-SEM SUPRA 40 Carl Zeiss, Germany) and high resolution transmission electron microscopy (HRTEM) using a JEOL JEM-2010F transmission electron microscope (TEM, JEOL Ltd, Japan) operating at 200 kV. TEM samples were prepared by dispersing a small amount of the sample in ethanol with the help of an ultrasonic bath. Small droplets of the freshly prepared dispersion were placed onto a copper grid covered with carbon to improve the conduction of the electrons. In addition, the surface area was estimated by the Brunauer–Emmett–Teller (BET) method using a Gemini VII 2390 instrument (Micromeritics, USA).

Measurement of photocatalytic activity

Photocatalytic efficiency for the degradation of RhB was carried out under the radiation of a 220 W OSRAM ultravitalux lamp (OSRAM, Germany), with a measured radiation intensity of 60 W/m^2 in the UV-A range. An aqueous solution with an initial volume of 150 mL was prepared with 0.05 g of catalyst and RhB 10 ppm, the solution was sonicated first for 30 min and then stirred in the dark for 30 min to ensure a good dispersion of TiO_2 particles and adsorption of RhB on the catalysts. Then, 4 mL samples of the suspension were taken just before illumination and after illumination at periods of 5 or 15 min. The samples were centrifuged at 10,000 rpm for 8 min using a 5804R Eppendorf Ultracentrifuge (Eppendorf, Germany) to separate the photocatalyst from the solution. The concentration of RhB in the solution was determined by UV-Vis spectroscopy. The evolution of the RhB concentration was determined as a function of the irradiation time from the change in absorbance at 564 nm. The efficiency of the nanotubes and nanorods was compared with their respective precursor TiO_2 powders.

RESULTS AND DISCUSSION

Figure 1 shows FE-SEM and TEM images of the SG-TiO_2 nanoparticles (NP). The images show that the NP displayed a radius of approximately 7 nm and formed relatively large and compact aggregates. Figure 2 shows the morphology and structure of the materials formed after 18 h of exposing the SG-TiO_2 powder to alkaline hydrothermal treatment. The images indicate that the NP turned to tube-like nanostructures with an average inner and external diameter of approximately 5.6 and 8 nm, respectively. After hydrothermal treatment, the samples were acid treated to replace Na^+ by H^+. Figure 2(b) shows that the tubular structure was conserved in spite of the acid treatment. Figure 2(c) shows the morphology and structure of the samples after annealing at 400 °C. The images clearly show that, as a consequence of annealing, the tube-like nanostructures turned

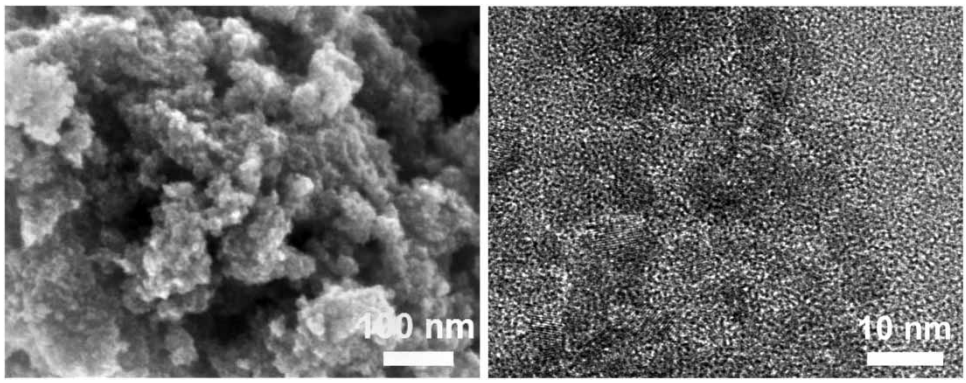

Figure 1 | FE-SEM and TEM images (left and right, respectively) for TiO_2 nanoparticles obtained by sol-gel method.

into short rod-like particles. Most of these particles remained attached to one another, resembling the original morphology of the tubes. These results suggest that during annealing, the structure of the tubes collapsed, cutting the tubes into smaller pieces but preserving in part their original morphology. Longer hydrothermal treatment was also performed, but no appreciable changes in morphology were detected. Figure 2(d) shows examples of tubular TiO_2 nanostructures obtained after 24 h of treatment.

Figure 3 shows TEM images of TiO_2 nanostructures obtained by alkaline hydrothermal treatment of P25-TiO_2 powder during 18 or 24 h, followed by acid exchange and 2 h annealing at 400 °C. As in the previous case, tubes were obtained in both hydrothermal treatment times (18 and 24 h). But in this case, the tubular 1D structure was maintained after annealing. The insets shown in Figure 3 are diffraction patterns obtained by fast Fourier transform (DPFFT). The patterns showed well-defined points, some corresponding to (101) plane distances typical of anatase.

The growth mechanism of 1D TiO_2 nanostructures synthesized by alkaline hydrothermal method from TiO_2 nanoparticles is still under discussion. It was suggested that it takes place by the rolling of hydrogen titanate laminar structures during the ion exchange step (Kasuga *et al.* 1998; Capula 2007), but other authors suggest that the 1D structure forms during the treatment of TiO_2 in NaOH aqueous solution (Du *et al.* 2001; Zhang *et al.* 2003, 2010). Our results seem to be in agreement with the latter authors because the tubes were well-formed before the acid treatment was applied.

Figure 4 shows the XRD patterns of nanoparticles obtained by the sol-gel method and the products obtained after hydrothermal treatment for 18 h, with further acid treatment and the final product obtained after annealing at 400 °C for 2 h. The SG-TiO_2 NP used as precursors showed an XRD pattern typical of low crystalline anatase. After hydrothermal treatment, the structure of the solid changed to another, displaying reflection peaks at 10, 24.5, 28.4 and 48.3 degrees 2θ. These peaks can be assigned to the diffraction of sodium titanates with the chemical formula $Na_2Ti_nO_{2n+1}$ ($n = 3$, 6, 9). In agreement with Joint Committee on Powder Diffraction Standards (JCPDS) N° 31–1329 and 33–1293, we could describe it as a mix of $Na_2Ti_3O_7$ and $Na_2Ti_9O_{19}$ designed as sodium titanates. After acid treatments, the features corresponding to titanate almost disappeared, being replaced by poorly defined peaks that may be associated with anatase. After the annealing process, only anatase the TiO_2 crystalline phase was observed since the samples showed well-defined peaks around 25.3, 37.8, 48.0 2θ degrees, characteristic of (101), (004) and (200), respectively of anatase TiO_2. It should be noted that before annealing, the samples were poorly crystalline since the X-ray reflections were slightly defined. After annealing, the crystal structure of the samples was well defined, in agreement with the DPFFT analysis (Figure 3). The crystalline structures correspond mainly to anatase, although a small amount of brookite could be detected in all cases. By analyzing the width at half maximum of the reflections employing Scherrer's equation, in the direction of (101) plane in Figure 4, crystallite sizes about 5 and 16 nm around were found for the SG-TiO_2-precursor and for the rod-like structures, respectively. This result shows that the crystallite size increased when the rod-like shape structures were formed. Table 1 shows the BET surface area values of the different samples. In the case of the TiO_2 nanostructures obtained from SG-TiO_2, there was a clear diminution of surface area as a consequence of the morphological transformation. These results suggest that the conversion from particles to nanorods occurred by a dissolution-precipitation process that involved

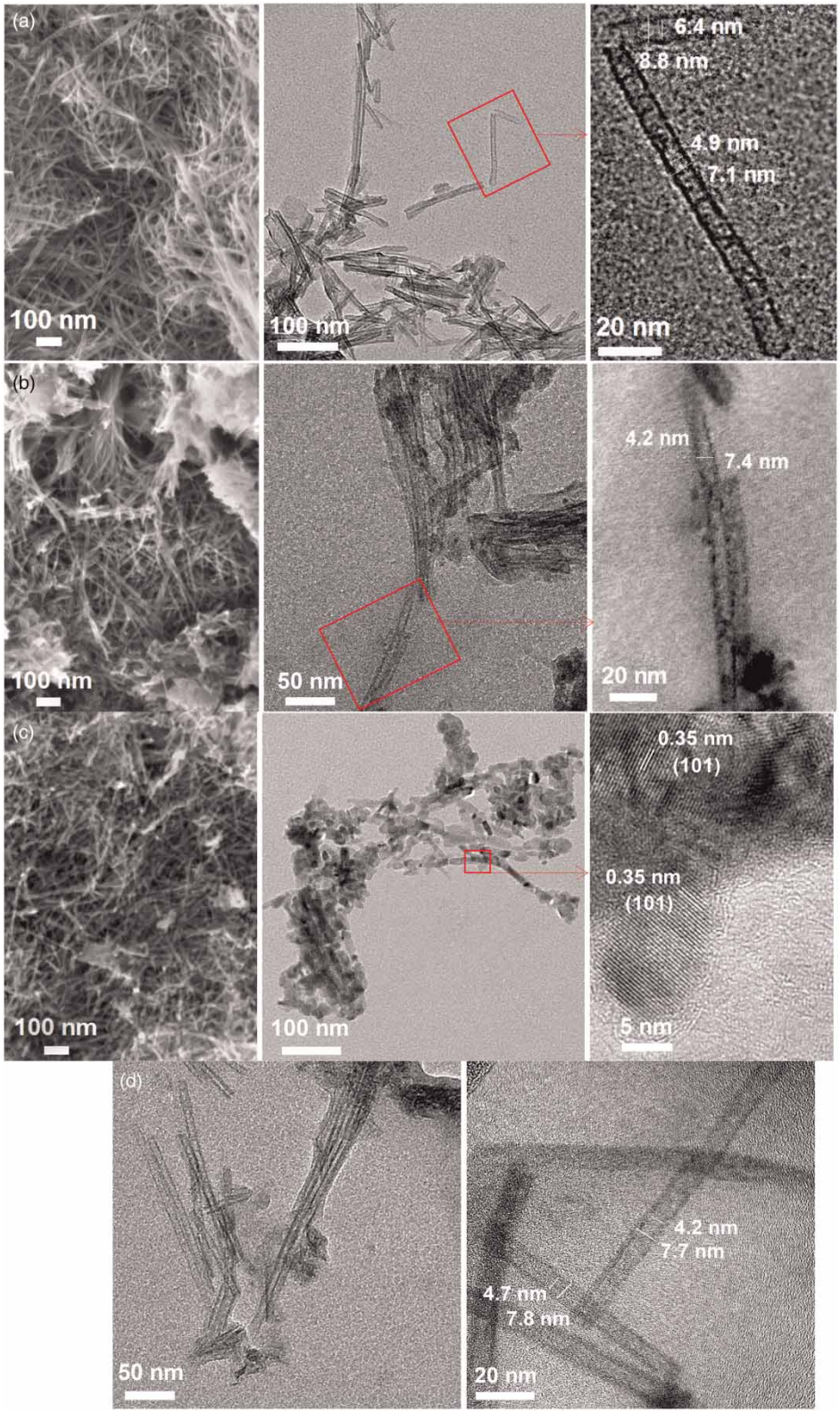

Figure 2 | FE-SEM and TEM images (left and right, respectively) of 1D nanostructures obtained from SG-TiO_2 powders, hydrothermally treated for 18 h (a), after acid treatment (b) and after annealing at 400 °C (c); TEM images of tubular TiO_2 nanostructures obtained after 24 h of hydrothermal treatment (d).

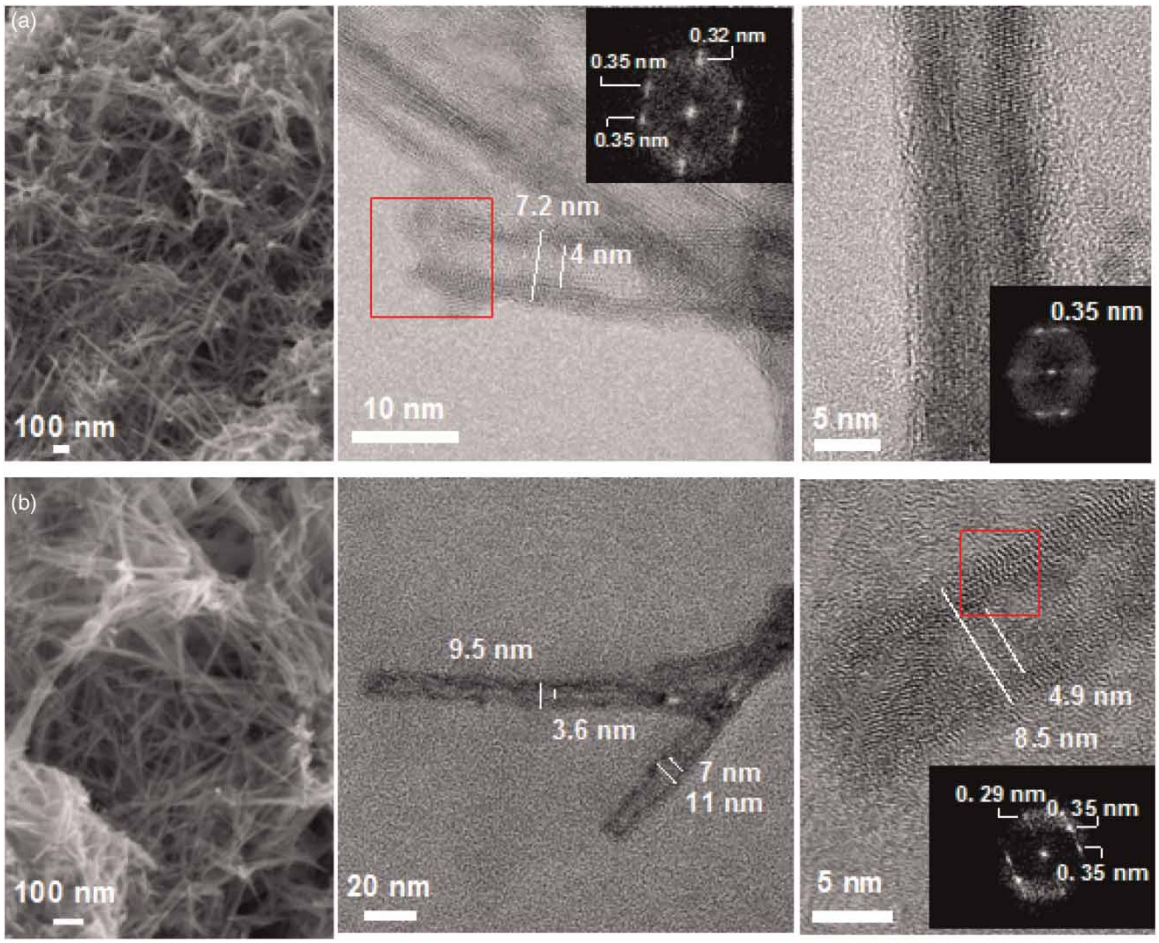

Figure 3 | FE-SEM and TEM images (left and right, respectively) of 1D nanostructures obtained from P25-TiO_2 powders hydrothermally treated for 18 h (a) and 24 h (b) with subsequent acid treatment and finally annealed at 400 °C. The insets are DPFFT of the area highlighted.

the transformation of TiO_2 to sodium titanate, followed by proton exchange to produce titanic acid and, finally, crystallization to anatase after thermal treatment. The crystalline structure evolved through all these steps, giving more crystalline compounds with a lower surface area.

Figure 5 shows XRD patterns of P25-TiO_2 powder and the TiO_2 nanostructures obtained after alkaline hydrothermal treatment, acid exchange and annealing at 400 °C. P-25 showed the typical reflection peaks corresponding to anatase and rutile. After hydrothermal treatment, the diffraction pattern shows peaks at 10, 24.5, 28.4 and 48.3 degrees 2θ. As discussed earlier, these features correspond to a mix of sodium titanate described by $Na_2Ti_3O_7$ and $Na_2Ti_9O_{19}$. After acid treatment, the intensity of 10 and 28.4 degree peaks was practically negligible, while the corresponding peak to 24.5 degrees increased to similar intensity as the 48 degree peak. These reflections are usually assigned as hydrogen titanates $H_2Ti_3O_7$ (Kolen'ko *et al.* 2006). It should be noted that both products display better-defined peaks than in the previous case. The main crystalline phase of the final annealed product was also anatase, but in contrast to the rod-shaped structures obtained from SG- TiO_2, the crystallite size for nanotubes was in the 8–10 nm range, which was much less than the crystallite size of the P-25-TiO_2: 21.5 nm. In addition, as shown in Table 1, the specific surface area of the P25-TiO_2 powders is much lower than its corresponding 1D TiO_2 nanostructures. The P-25 seeds are more crystalline than the nanostructures obtained by hydrothermal treatment and even displayed some amount of rutile. This difference is due to the high temperature synthesis used in the preparation of P25-TiO_2. Clearly, the P25-TiO_2 particles were also exposed to dissolution-precipitation processes that lead to the disappearance of the rutile phase. The new solid phases displayed a more disorganized structure with lower crystallite sizes and higher surface area than the precursor powder. It is remarkable that in this system the nanotubes

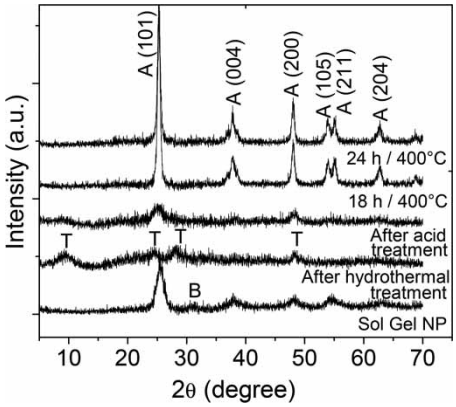

Figure 4 | XRD patterns of sol-gel nanoparticles (NP) and the product obtained from it after 18 h of hydrothermal treatment, sample with further acid treatment and finally annealed at 400 °C (18 h/400 °C). The final product obtained with 24 h of hydrothermal treatment is also shown (24 h/400 °C) (A = anatase, B = brookite, T = sodium titanate).

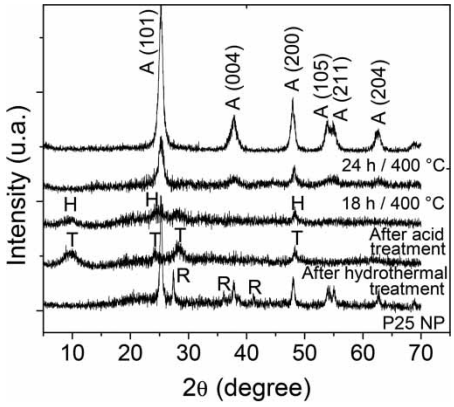

Figure 5 | XRD patterns of P25-TiO_2 powder and the product obtained from it after 24 h of hydrothermal treatment, sample with further acid treatment and finally annealed at 400 °C (24 h/400 °C). The final product obtained with 18 h of hydrothermal treatment is also shown (18 h/400 °C) (A = anatase, R = rutile, T = sodium titanate, H = hydrogen titanate).

Table 1 | BET surface area of the different samples

TiO_2 nanostructures	Surface area BET (m^2/g)	TiO_2 nanostructures	Surface area BET (m^2/g)
TiO_2 NPs-Sol Gel	201	TiO_2 P 25 NPs	60
1D Nanostructures 18 h/400 °C[a]	97	1D Nanostructures 18 h/400 °C[a]	279

[a]Hydrothermal treatment time/annealing temperature.

did not collapse after annealing, preserving the high surface area. Although the reasons are still not clear, it was reported that the thermal and structure stability depend on the type of precursor (Preda *et al.* 2013). The low thermal stability of the TiO_2 NP, may be a consequence of the presence of anatase seeds after acid washing. These seeds may trigger the crystallization of anatase, leading to the rearrangement and collapse of the structure.

The photocatalytic activities of the obtained samples were tested via degradation of aqueous RhB under UVA irradiation. It is important to note that in the literature it is very common to report the beginning of the degradation curve as 0% of degradation at 0 time. However, adsorption on the photocatalyst should be considered. In this case the degradation curve was drafted considering the initial decrease of RhB due to adsorption of the dye onto TiO_2 photocatalyst. As shown in Figures 6 and 7 before the irradiation ($t = 0$), an adsorption process of RhB onto the TiO_2 nanostructures was observed. The adsorption onto commercial P25-TiO_2 was measured to be 4% and 5 and 2% for final 1D structures obtained with 18 and 24 h of hydrothermal treatment, respectively. Conversely, absorption was approximately 1 and 2% for samples obtained from SG-TiO_2 after 18 and 24 h of thermal treatment, respectively, and practically negligible for the SG-TiO_2 precursor. The adsorption amount could be ascribed to the high surface area of the TiO_2 nanotubes and nanorods.

Figure 6 shows the evolution of RhB concentration in UVA illuminated solution containing TiO_2 nanotubes obtained from P-25. The results indicate that the annealed nanotubes display much higher photocatalytic activity than the raw nanotubes. This phenomenon can be associated with the different nature of the TiO_2 nanotubes before and after annealing. Only after firing did the structure of the nanotubes become anatase (see Figure 5), which is the crystalline TiO_2 phase with well-known photocatalytic activity.

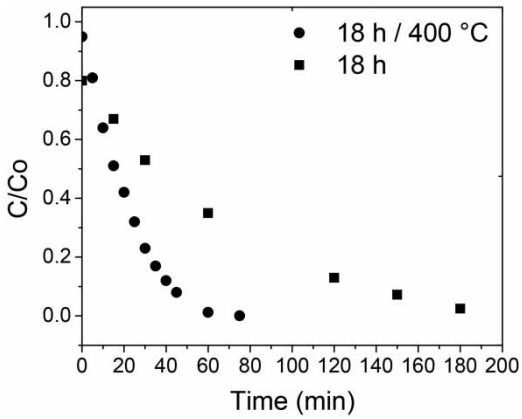

Figure 6 | RhB degradation for sample obtained from P25 hydrothermally treated for 18 h with further acid treatment (■) and after annealing process at 400 °C (•).

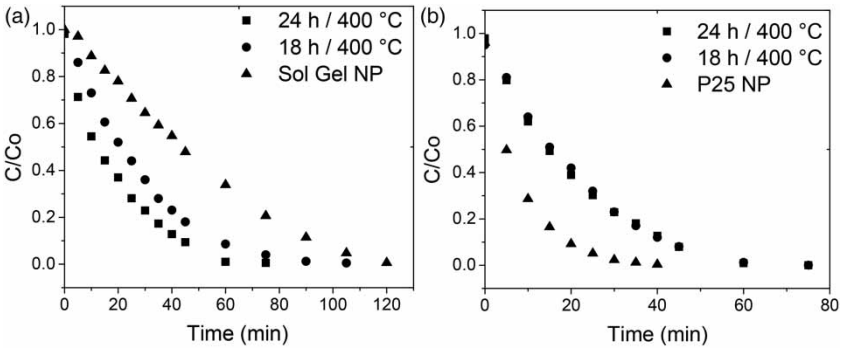

Figure 7 | Degradation of RhB solutions with sol-gel nanoparticles and the 1D nanostructures obtained from it (a) and P25 nanoparticles and the 1D nanostructures obtained from it (b).

Figure 7(a) shows the photocatalytic degradation of RhB in solutions containing SG-TiO_2 NP, and annealed 1D TiO_2 obtained from TiO_2-SG NP precursor. Clearly, the photocatalytic activity of the 1D TiO_2 samples is higher than that displayed by the precursor material, being more active than the sample exposed to longer hydrothermal treatment. This phenomenon can be a consequence of the different crystallite sizes displayed by the systems. It was reported that a highly crystalline structure leads to more active photocatalysts due to a diminution in the recombination of the photogenerated carriers (Liu *et al*. 2014). In this case, as shown in Figure 4, the annealed nanotubes displayed a well-crystallized anatase structure. Figure 7(b) allows comparison of the photocatalytic activity of P-25 with the activity of 1D TiO_2 obtained by hydrothermal treatment of P-25 followed by annealing. In this case, the precursor material displayed higher photocatalytic activity than the 1D TiO_2 structures, even though the 1D nanostructures had a larger surface area. This result may be a consequence of different phenomena. For instance, it was proposed that the presence of both crystalline phases (anatase and rutile) in the P25-TiO_2 particles may improve the photocatalytic response of this material (Su *et al*. 2011). Alternatively, the crystalline domains of the 1D TiO_2 nanostructures are quite small (6–11 nm) hindering the photo activity of the material. This effect may be a consequence of the presence of dangling bonds or distorted lattice structures that may act as electron-hole recombination sites (Henderson 2011). Moreover, the 1D nanostructures were not pure in morphology but were mixed with particles of different shapes and even amorphous TiO_2. Despite the 1D nanostructures showing lower photocatalytic activity than P25-TiO_2, these nanostructures displayed a reasonably good photocatalytic activity for RhB degradation since we achieved the complete degradation of a concentrate solution in 60–80 min (shorter than reported by other authors (Zhang *et al*. 2010; Thennarasu *et al*. 2013)).

CONCLUSIONS

TiO_2 anatase 1D nanostructures, with high surface area and photocatalytic activity, were synthesized by hydrothermal treatment. The structure of the systems depended on the TiO_2 precursor powder used in the synthesis. P25-TiO_2 produced nanotubes that were not altered by the thermal treatment, but the structures produced from SG-TiO_2 collapsed after annealing at 400 °C. This phenomenon may be a consequence of the presence of anatase seeds in the TiO_2 nanotubes after acid washing. All the synthesized 1D TiO_2 nanostructures were effectively used in the photocatalytic degradation of Rhodamine B. The efficiency of the TiO_2 nanotubes as a photocatalyst was lower than that of P-25 (under similar conditions), although it was still high enough to be successfully used as a photocatalyst. It should be mentioned that the rod-like nanostructures displayed higher efficiency than those from the SG TiO_2 precursor. The lower photocatalytic activity of the nanostructures with respect to P25 can be related to the lower crystallinity of 1D TiO_2 in both materials and the absence of rutile as minor phase. Due to its photocatalytic activity, aspect ratio and tubular structure, this material is very attractive as a component for the synthesis of functional materials for environmental applications. For example, TiO_2 nanotubes could be used to prepare filtration membranes with self-cleaning properties under UVA illumination (preventing membrane fouling). TiO_2 nanotubes are also more easily filterable than NP and can be easily removed from solutions. Hence, the possibility to produce a photocatalytic material with different shapes makes

it more versatile for photocatalytic application by itself or in the form of composite materials.

ACKNOWLEDGEMENTS

This work was supported by the Fincyt Project No 140-FINCYT-IB-2013, the Peruvian-Argentinean 2011–02-CONCYTEC OAJ Project and MINCYT-CONCYTEC PE/11/02, CONICET-PIP 112–200801–02533, UBACYT Nos. 20020100100350 and 20020090100297 and the Pacific Alliance Program 2013–2 through the SRE-México. RJC is member of CONICET. We are grateful to the Central Laboratory of Microscopy of Physic Institute of UNAM from Mexico.

REFERENCES

Adachi, M., Murata, Y., Okada, I. & Yoshikawa, S. 2003 Formation of titania nanotubes and applications for dye-sensitized solar cells. *J. Electrochem. Soc.* **150** (8), G488–G493.

Asiah, M. N., Mamat, M. H., Khusaimi, Z., Achoi, M. F., Abdullah, S. & Rusop, M. 2013 Thermal stability and phase transformation of TiO_2 nanowires at various temperatures. *Microelectron. Eng.* **108**, 134–137.

Capula, S. 2007 Synthesis, characterization and photocatalytic activity evaluations of Pt-Ir nanoparticles supported onto titania nanotubes. Master in Science Thesis, Instituto Politécnico Nacional, Mexico D.F., Mexico.

Cowan, A., Tang, J., Leng, W., Durrant, J. & Klug, D. 2010 Mechanism of water splitting by TiO_2. *J. Phys. Chem. C* **114** (9), 4208–4214.

Du, G. H., Chen, Q., Che, R. C., Yuan, Z. Y. & Peng, L. M. 2001 Preparation and structure analysis of titanium oxide nanotubes. *Appl. Phys. Lett.* **79** (22), 3702–3704.

Henderson, M. A. 2011 A surface science perspective on TiO_2 photocatalysis. *Surf. Sci. Rep.* **66**, 185–297.

Ibhadon, A. O. & Fitzpatrick, P. 2013 Heterogeneous photocatalysis: recent advances and applications. *Catalysts* **3**, 189–218.

Kasuga, T., Hiramatsu, M., Hoson, A., Sekino, T. & Niihara, K. 1998 Formation of titanium oxide nanotube. *Langmuir* **14** (12), 3160–3163.

Kolen'ko, Y. V., Kovnir, K. A., Gavrilov, A. I., Garshev, A. V., Frantti, J., Lebedev, O. I. & Yoshimura, M. 2006 Hydrothermal synthesis and characterization of nanorods of various titanates and titanium dioxide. *J. Phys. Chem. B* **110** (9), 4030–4038.

Lai, C. W., Juan, J. C., Bae Ko, W. & Abd Hamid, S. B. 2014 An overview: recent development of titanium oxide nanotubes as photocatalyst for dye degradation. Publishing Corporation. *Int. J. Photoenergy* **2014**, 14, Article ID 524135.

Liu, N., Chen, X., Zhang, J. & Schwank, J. W. 2014 A review on TiO_2-based nanotubes synthesized via hydrothermal method: Formation mechanism, structure modification, and photocatalytic applications. *Catal. Today* **225**, 34–51.

Maiyalagan, T., Viswanathan, B. & Varadaraju, U. 2006 Fabrication and characterization of uniform TiO_2 nanotube arrays by sol-gel templating method. *Bull. Mater. Sci.* **29** (7), 705–708.

Nakahira, A., Kubo, A. & Numako, C. 2010 TiO_2-derived titanate nanotubes by hydrothermal process with acid treatments and their microstructural evaluation. *Appl. Mater. Interfaces* **2** (9), 2611–2616.

Neupane Madhav, P., Song Park, I., Sung Bae, T., Keun Yi, H., Watari, F. & Ho Lee, M. 2011 Synthesis and morphology of TiO_2 nanotubes by anodic oxidation using surfactant based fluorinated electrolyte. *J. Electrochem. Soc.* **158** (8), C242–C245.

Ollis, D. F., Pelizetti, E. & Serpone, N. 1991 Destruction of water contaminants. *Environ. Sci. Technol.* **25**, 1522–1529.

Preda, S., Teodorescu, V. S., Musuc, A. M., Andronescu, C. & Zaharescu, M. 2013 Influence of the TiO_2 precursors on the thermal and structural stability of titanate-based nanotubes. *J. Mater. Res.* **28** (03), 294–303.

Ren, Y., Zheng, L., Pourpoint, F., Armstrong, A., Grey, C. & Bruce, P. 2012 Nanoparticulate TiO_2 (B): anode for lithium-ion batteries. *Angew. Chem. Int. Ed.* **51**, 2164–2167.

Su, R., Bechstein, R., Sø, L., Vang, R. T., Sillassen, M., Palmqvist, A. & Besenbacher, F. 2011 How the anatase-to-rutile ratio influences the photoreactivity of TiO_2. *J. Phys. Chem.* **115** (49), 24287–24292.

Thennarasu, S., Rajasekar, K. & Balkis Ameen, K. 2013 Hydrothermal temperature as a morphological control factor: Preparation, characterization and photocatalytic activity of titanate nanotubes and nanoribbons. *J. Mol. Struct.* **1049**, 446–457.

Wang, D., Zhou, F., Liu, Y. & Liu, W. 2008 Synthesis and characterization of anatase TiO_2 nanotubes with uniform diameter from titanium powder. *Mater. Lett.* **62**, 1819–1822.

Wu, J. J. & Yu, C. C. 2004 Aligned TiO_2 nanorods and nanowalls. *J. Phys. Chem. B* **108** (11), 3377–3379.

Yamin, Y., Keller, N. & Keller, V. 2012 WO_3-modified TiO_2 nanotubes for photocatalytic elimination of methylethylketone under UVA and solar light irradiation. *J. Photochem. Photobiol. A: Chem.* **245**, 43–57.

Yan, J. & Zhou, F. 2011 TiO_2 nanotubes: Structure optimization for solar cells. *J. Mater. Chem.* **21**, 9406.

Zhang, R., Tu, B. & Zhao, D. 2010 Synthesis of highly stable and crystalline mesoporous anatase by using a simple surfactant sulfuric acid carbonization method. *Chem. Eur. J.* **16**, 9977–9981.

Zhang, Z. J., Zhang, J. W., Guo, X. Y., Jin, Z. S., Zhang, S. L. & Zhou, J. F. 2003 TEM study on the formation process of TiO_2 nanotubes. *Chin. Chem. Lett.* **14** (4), 419–422.

First received 28 February 2014; accepted in revised form 30 June 2014. Available online 12 July 2014